Analog and digital simulations of Maxwellian plasmas for astrophysics[1]

D.W. Savin, N.R. Badnell, P. Beiersdorfer, B.R. Beck, G.V. Brown, P. Bryans, T.W. Gorczyca, M.F. Gu, S.M. Kahn, J.M. Laming, D.A. Liedahl, W. Mitthumsiri, J.H. Scofield, and K.L. Wong

Abstract: Many astrophysical and laboratory plasmas possess Maxwell–Boltzmann (MB) electron energy distributions (EEDs). Interpreting or predicting the properties of these plasmas requires accurate knowledge of atomic processes such as radiative lifetimes, electron impact excitation and de-excitation, electron impact ionization, radiative recombination, dielectronic recombination, and charge transfer, all for thousands of levels or more. Plasma models cannot include all of the needed levels and atomic data. Hence, approximations need to be made to make the models tractable. Here we report on an "analog" technique we have developed for simulating a Maxwellian EED using an electron beam ion trap and review some recent results using this method. A subset of the atomic data needed for modeling Maxwellian plasmas relates to calculating the ionization balance. Accurate fractional abundance calculations for the different ionization stages of the various elements in the plasma are needed to reliably interpret or predict the properties of the gas. However, much of the atomic data needed for these calculations have not been generated using modern theoretical methods and are often highly suspect. Here we will also review our recent updating of the recommended atomic data for "digital" computer simulations of MB plasmas in collisional ionization equilibrium (CIE), describe the changes relative to previously recommended CIE calculations, and discuss what further recombination and ionization data are needed to improve this latest set of recommended CIE calculations.

PACS Nos.: 34.70.+e,34.80.Dp, 34.80.Kw, 34,80,Lx, 52.50.−j, 52.20.Fs, 52.20.Hv, 52.25.Jm, 52,72.+v, 52.75.−d, 95.30.Dr, 95.30.Ky, 98.38.Bn, 98.58.Bz

Résumé : Dans beaucoup de plasmas en astrophysique et au laboratoire nous trouvons une distribution de Maxwell–Boltzmann (MB) pour l'énergie des électrons (EED). Pour interpréter ou prédire les propriétés de ces plasmas, nous avons besoin de connaître de façon précise certains mécanismes atomiques, comme les temps de vie radiatifs, la recombinaison radiative, la recombinaison diélectrique et le transfert de charge pour des milliers de niveaux et encore. Les modèles du plasma ne peuvent pas inclure tous les niveaux et les données atomiques nécessaires. Nous devons alors faire des approximations pour que le modèle reste utilisable. Nous présentons une technique *analogique* que nous avons développée pour simuler une EED maxwellienne en utilisant un piège ionique a faisceau d'électrons et passons en revue des résultats récents obtenus en utilisant cette approche. Un sous-ensemble des données atomiques requises pour la modélisation maxwellienne des plasmas est relié au calcul de la balance d'ionisation. Nous avons besoin de calculs précis d'abondances fractionnaires pour les différents stages d'ionisation des différents éléments dans le plasma afin de prédire ou d'interpréter de façon fiable les propriétés du gaz. Cependant, la majeure partie des données atomiques requises pour ces calculs n'a pas été générée par des méthodes théoriques modernes et est souvent de qualité discutable. Nous passons ici en revue notre récente mise à jour des données atomiques requises pour des simulations *numériques* sur ordinateur de plasmas MB en équilibre ionique collisionnel (CIE), décrivons les changements avec les précédents calculs CIE et discutons quelles données additionnelles de recombinaison et d'ionisation sont requises pour améliorer le dernier ensemble de calculs CIE.

[Traduit par la Rédaction]

Received 16 February 2007. Accepted 25 April 2007. Published on the NRC Research Press Web site at http://cjp.nrc.ca/ on 7 February 2008.

D.W. Savin,[2] P. Bryans, and W. Mitthumsiri. Columbia Astrophysics Laboratory, Columbia University, New York, NY 10027, USA
N.R. Badnell. Department of Physics, University of Strathclyde, Glasgow, G4 0NG, UK.
P. Beiersdorfer, B.R. Beck, G.V. Brown, M.F. Gu, D.A. Liedahl, J.H. Scofield, and K.L. Wong. Lawrence Livermore National Laboratory, Livermore, CA 94550, USA.
T.W. Gorczyca. Department of Physics, Western Michigan University, Kalamazoo, MI 49008, USA.
S.M. Kahn. Kavli Institute for Particle Astrophysics and Cosmology, Stanford Linear Accelerator Center and Stanford University, 2575 Sand Hill Road, Menlo Park, CA 94025, USA.
J.M. Laming. E. O. Hulburt Center for Space Research, US Naval Research Laboratory, Code 7674L, Washington, DC 20375, USA.

[1]Paper given at the Workshop on Twenty Years of Spectroscopy with EBIT held in Berkeley, California, 13–15 November 2006.
[2]Corresponding author (e-mail: savin@astro.columbia.edu).

 doi: 10.1139/P07-159

1. Maxwell–Boltzmann (MB) plasmas

Plasmas with a Maxwell–Boltzmann (MB) electron energy distribution (EED) are ubiquitous. In the cosmos they are observed in the sun and other stars, supernova remnants, galaxies, and the intercluster medium of clusters of galaxies. In the laboratory MB plasmas are found in fusion devices, Z-pinches, laser produced plasmas, and many other sources.

Interpreting or predicting the properties of MB plasmas is challenging. Atomic data are needed for thousands upon thousands of processes. Experiments can provide only a fraction of the needed data. Theory provides the bulk of the data, but approximations need to be made to keep the calculations tractable. Also, plasma models cannot include all the needed data without becoming computationally prohibitive.

One solution to this problem of understanding MB plasmas is to effectively build an analog computer in the laboratory. This can be done by creating an MB plasma under controlled conditions to benchmark plasma models. This tests everything at once, both the plasma model and the underlying atomic data.

Tokamaks, θ pinches, Z pinches, and laser produced plasmas are some of the commonly laboratory devices used to study MB plasmas, and a large amount of research has been carried out using these devices (for example, see the many articles in refs. 1–5). However, the accuracy of such research is often limited by complications such as density effects, radiative transfer, ion abundance gradients, the electron temperature and density structure of the plasma, and line-of-sight averaging of the observed photon emission over regions of multible electron temperatures. As is discussed later and in ref. 6, we have developed a laboratory method that is complementary to the commonly used laboratory devices to study MB plasmas, but which does not suffer from the complications associated with those approaches.

Here we report on work that we have carried out over the last decade to improve our understanding of MB plasmas. In Sect. 2, we describe the method we have developed to use the nearly monoenergetic electron beam in an electron beam ion trap (EBIT) to simulate an MB plasma. This technique was first implemented on the EBIT-II electron beam ion trap at Lawrence Livermore National Laboratory [7] and has recently been adapted to the Livermore EBIT-I device. Our initial tests of the fidelity of the MB simulations are described in Sect. 3. Sections 2 and 3 are summaries of the more detailed discussion of our EBIT MB "analog" simulation work given in ref. 6.

An important property of steady-state MB plasmas is the collisional ionization equilibrium (CIE) reached in the plasma. In Sect. 4, we discuss previous work that has been carried out to calculate fractional ionic abundances for astrophysical MB plasmas in CIE. Our recent improvements to CIE calculations and some results are also presented in this section. MB studies at the Livermore EBITs have recently been expanded to investigate CIE as noted in Sect. 5. We conclude this paper with a discussion of the future atomic data needs for improving our understanding of MB plasmas in CIE. Additional discussion of these "digital" simulations of MB plasmas in CIE are given in ref. 8.

2. Simulating MB plasmas in an electron beam ion trap

2.1. Simulating an MB energy distribution

The key to simulating an MB plasma using the nearly monoenergetic beam in an EBIT is to sweep the electron beam energy E in time so that,

$$\frac{\mathrm{d}\tau}{\tau_o} = P(E, T_\mathrm{e})\,\mathrm{d}E \tag{1}$$

where τ_o is the time length of sweep period, τ is the time in this period, and $P(E, T_\mathrm{e})$ is the MB probability at an electron temperature T_e of finding an electron in the energy range E to $E + \mathrm{d}E$. Here, we have implicitly assumed that the electron density n_e is kept constant. The MB probability is given by,

$$P(E, T_\mathrm{e})\,\mathrm{d}E = \frac{2E^{1/2}}{\pi^{1/2}(k_\mathrm{B}T_\mathrm{e})^{3/2}} \exp\left(\frac{-E}{k_\mathrm{B}T_\mathrm{e}}\right) \mathrm{d}E \tag{2}$$

where k_B is the Boltzmann constant. As is described in ref. 6, solving for τ yields

$$\tau(E) = \tau_o \left[\mathrm{erf}(x) - \frac{2x\mathrm{e}^{-x^2}}{\sqrt{\pi}}\right] \tag{3}$$

where $\mathrm{erf}(x)$ is the error function, $x = (E/k_\mathrm{B}T_\mathrm{e})^{1/2}$, and the quantity in the square brackets ranges between 0 and 1. The electron energy sweep pattern $E(\tau)$ may be calculated numerically using (3).

2.2. Maintaining a constant-density electron beam

The electron density is kept constant as E is swept for a number of reasons. This keeps space charge and trapping conditions largely unchanged during the sweeping. It also helps to maintain a constant electron–ion overlap versus beam energy. This last point is important as it helps to ensure all electron–ion collision processes go forward at the correct plasma rates.

The current from a Pierce electron gun, such as is used in the Livermore EBITs, is given by [9],

$$I_\mathrm{e} = pV_\mathrm{a}^{3/2} \tag{4}$$

where p is the perveance in units of amperes volts$^{-3/2}$ and V_a is anode voltage in volts. For a beam with a shape and size constant with E, we have

$$n_\mathrm{e} \propto \frac{I_\mathrm{e}}{v_\mathrm{e}} \propto \frac{V_\mathrm{a}^{3/2}}{E^{1/2}} \tag{5}$$

where v_e is the electron beam velocity at energy E. To keep n_e constant as a function of $E(\tau)$, V_a is swept so that

$$V_\mathrm{a}(\tau) = (V_\mathrm{a})_\mathrm{r}\left[\frac{E(\tau)}{E_\mathrm{r}}\right]^{1/3} \tag{6}$$

where $(V_\mathrm{a})_\mathrm{r}$ is the anode voltage at an arbitrary reference energy E_r.

2.3. Technical limitations

Technical limitations constrain the implementation of the MB simulation in an EBIT. The most obvious of these are the minimum and maximum energies, $E_{\min}$ and $E_{\max}$, respectively, between which the beam energy can be swept. For the Livermore EBITs, typically $E_{\min} \gtrsim 0.2$ keV. Although measurements can be performed with lower beam energies [10], the electron beam is poorly behaved for these lower energies and does not lend itself to automated control with rapidly varying conditions. This is not expected to be a significant problem for studying X-ray emitting plasmas as most collision processes of interest occur for $E > 0.2$ keV.

Values of $E_{\max}$ are typically kept to $\leq$ (5–6)$k_{\rm B}T_{\rm e}$. This is due to capacitances limiting $\mathrm{d}E/\mathrm{d}t$ and $\mathrm{d}V_{\rm a}/\mathrm{d}t$ to $\leq$30 V/μs in the Livermore EBIT machines. As a result, the highest energy electrons in the MB distribution are not sampled. These constitute typically $\leq$2% of the total EED.

Because of the $E_{\min}$ and $E_{\max}$ limitation, we do not sweep over the entire period τ_o. The actual sweep period is given by $t_o = \tau(E_{\max}) - \tau(E_{\min})$. The specific time versus E in the applied sweep pattern $E(t)$ is given by $t(E) = \tau(E) - \tau(E_{\min})$.

To avoid problems of trying to sweep faster than the slew rate of the EBIT electrical system, we sweep from $E_{\min}$ to $E_{\max}$ and then back down to $E_{\min}$, using the same pattern as the upsweep but mirrored around $t = t_o$. For the $T_{\rm e}$ range we are interested in simulating, the maximum slew rate for E limits t_o to values $\gtrsim$5 ms.

Additionally, the space charge effects of the electron beam and trapped ions on the actual electron energy in the trap need to be estimated and corrected for (a correction typically on the order of 50–100 V). Lastly, the electron beam energy needs to be swept faster than the time scale over which the collision processes of interest occur. This is necessary to insure that the trapped ions see an actual MB EED (albeit a time-averaged one). Typical sweep times are on the order of 5 ms.

2.4. Representative sweep patterns

Figure 1 shows the sweeping pattern used to simulate an MB plasma of $k_{\rm B}T_{\rm e} = 2.4$ keV. Operating conditions were used with $E_{\min} = 0.6$ keV, $E_{\max} = 12.24$ keV, $(V_{\rm a})_{\min} = 1.2$ kV, and $t_o = 5$ ms. The sweep pattern rises smoothly up from $E_{\min}$ to $E_{\max}$ and smoothly back down to $E_{\min}$. We avoid jumping from $E_{\max}$ immediately back down to $E_{\min}$ because of the limited slew rates for E and $V_{\rm a}$ described earlier. Figure 2 shows the derivatives of the slew rates plotted in Fig. 1. $E_{\max}$ has been chosen to keep $\mathrm{d}E/\mathrm{d}t < 30$ V $\mu\mathrm{s}^{-1}$.

3. Fidelity of the MB simulations

To verify the accuracy of our simulated MB EEDs, we have carried out measurements of line emission due to dielectric recombination (DR) and electron impact excitation (EIE) of heliumlike neon, magnesium, and argon. Heliumlike ions are commonly used to measure $T_{\rm e}$ of a plasma by taking the ratio of DR produced lines to EIE lines [11].

Figure 3 shows how we were able to test the fidelity of the simulated MB EED. The ratio of line emission due to the DR resonance line known as j relative to the electron impact excitation line known as w can be used as a temperature diagnostic. Here, we use the notation of ref. [12]. The j line samples the EED at a single energy, while w integrates the EED from the

Fig. 1. Digitized timing pattern of the electron beam energy (top) and of the electron gun anode voltage (bottom) used for simulating a Maxwellian plasma at $k_{\rm B}T_{\rm e} = 2.4$ keV. Representative operating conditions of $E_{\min} = 0.6$ keV, $E_{\max} = 12.24$ keV, $(V_{\rm a})_{\min} = 1.2$ kV, and $t_o = 5$ ms have been used.

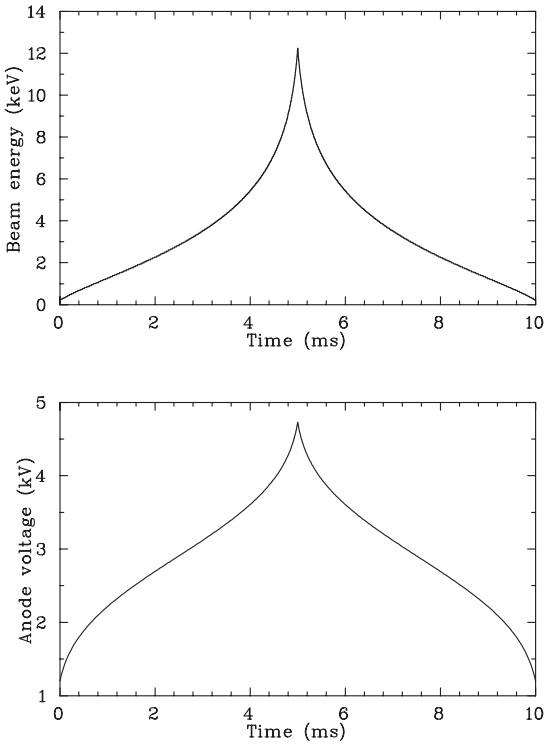

Fig. 2. Derivatives of the timing patterns shown in Fig. 1

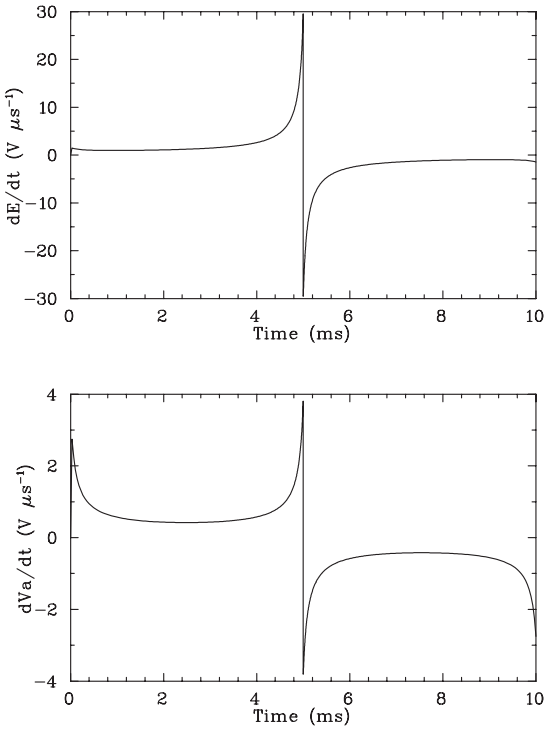

Fig. 3. The broken-line curve shows a Maxwell–Boltzmann electron energy distribution for $k_B T_e = 2.4$ keV. The continuous curve shows the electron energy that is swept out in the simulation generated using the pattern shown in Fig. 1 (spanning from 0.60 to 12.24 keV). The vertical dotted line shows the electrons contributing to the resonance line labeled as j, which is due to DR onto heliumlike ions. The filled-in area under the curve shows the electrons contributing to EIE of w, which is the resonance line of heliumlike ions. The ratio of line emission due to j and w is temperature sensitive. The energies for j and w shown here are for Ar^{16+}. See text and ref. 6 for additional details.

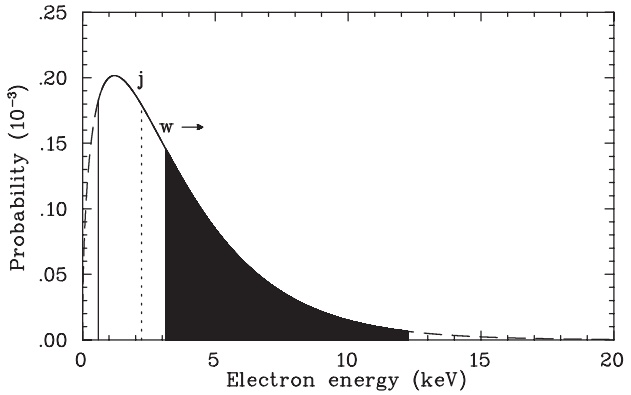

EIE threshold and up. As the temperature changes, so do the portions of the MB EED sampled. Thus, as the temperature of the plasma changes, the j/w ratio correspondingly changes [11].

A representative scatter plot of MB data taken on EBIT-II is shown in Fig. 4 for Mg^{10+} at a simulated temperature of $k_B T_e = 0.7$ keV. Extracting the integrated line intensities for j and w for a number of different simulated temperatures yields data such as that shown in Fig. 5. We can then turn around and use the experimental and theoretical data shown in Fig. 5 to infer the MB temperature based on the measured j/w ratio and the range of theoretical predictions for this ratio. Figure 6 shows the resulting spectroscopically inferred temperature versus the simulated temperature at which the data were collected. We find excellent agreement between the simulated and inferred electron temperatures. The inferred temperatures agree on average to within better than 10% with the simulated temperatures.

4. Collisional ionization equilibrium (CIE) calculations

CIE occurs in plasmas which are optically thin to radiation, of low enough density that three-body recombination is unimportant, dust-free so recombination on grains is not an issue, and in steady state or nearly so. Under these conditions the electron impact ionization (EII) rate equals the electron–ion recombination rate. Hence, the accuracy of these rates determines the reliability of the fractional ionic abundances calculated by a CIE model.

In astrophysics, plasmas in CIE are found in the Sun and other stars, galaxies, and the intercluster medium in clusters of galaxies. An early set of CIE calculations for astrophysical modeling are those of Shull and van Steenberg [18] who compiled published DR, radiative recombination (RR), and EII data.

Fig. 4. Scatter plot of photon wavelength versus electron beam energy for an MB simulation of $k_B T_e = 0.7$ keV. The vertical features above $E \sim 1.35$ keV are due to EIE of Mg^{10+} and are (using the notation of ref. 12) w, x, and y, which are blended, and z. The features at $E \sim 0.98$ keV are due to DR into the $n = 2$ level of Mg^{9+}. The features at $E \sim 1.2$ keV are DR into the $n = 3$ level. The tail on w below the EIE threshold energy is due to $n \geq 4$ DR.

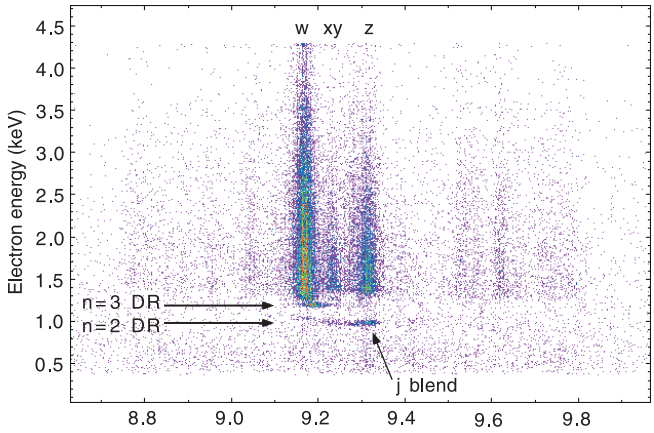

Fig. 5. Measured and theoretical j/w line ratio vs. $k_B T_e$ for magnesium. Experimental results are shown with their estimated 1σ confidence limits. In calculating the j/w line ratio, we used DR resonance strengths from refs. 13–15 and rate coefficients for w from refs. 6, 16, 17. The continuous-line curve is the theoretical line ratio derived using the average of these published theoretical data for j and w. The dotted curves represent the maximum and minimum theoretical line ratio based on the theoretical results in the literature and does not represent a 1σ uncertainty.

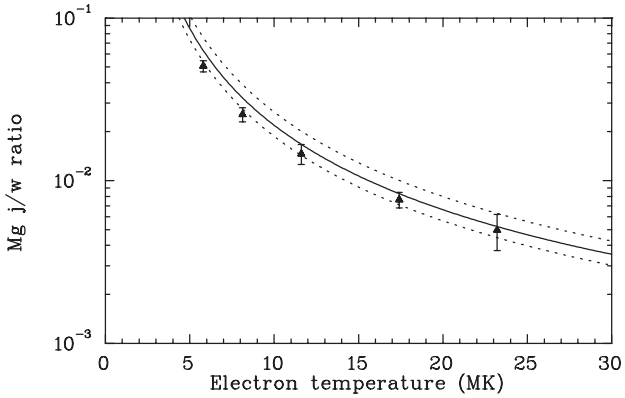

These data were updated by Arnaud and Rothenflug [19] and then again by Arnaud and Raymond [20], specifically for iron. Subsequently Mazzotta et al. [21] re-evaluated and updated the recombination data used in the models.

Since the work of Mazzotta et al. and particularly in the past four years, there have been significant theoretical advances in the DR and RR data available for modeling cosmic plasmas (as discussed in ref. 8). Modern DR and RR calculations have now been carried out for K-shell, L-shell, and Na-like ions of all elements from hydrogen up to and including zinc. For a given ion of a given element, modern theoretical calculations

Fig. 6. Spectroscopically inferred $k_B T_e$ (using j/w) plotted as a function of the simulated MB temperature. Data are shown for neon (squares), magnesium (triangles), and argon (circles). The error bars represent the combined effects of the 1σ experimental uncertainties and the range of theoretical j/w ratios. The straight line shows where the inferred and simulated temperatures are equal.

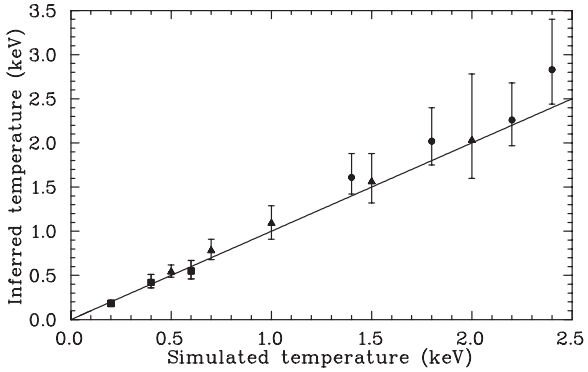

from different groups typically agree with one another to within 25% at the temperatures where that ion forms in CIE. This formation zone is defined here as the temperature range where the fractional ionic abundance is $\geq$1% of the total elemental abundance.

Laboratory measurements have been used to benchmark modern DR calculations. K-shell ions have been well studied using EBITs and ion storage rings. The agreement between theory and experiment is generally within ~20% [22, 23]. L-shell ions are less well studied and the agreement between theory and experiment is ~35% [8, 24, 25]. But as discussed later, further studies are needed. Additionally, DR theory is much less reliable at $\sim 10^4$ K ($k_B T_e \sim 1$ eV). This is because for the DR resonances important in 10^4 K plasmas, the uncertainties in the theoretical resonance energies can be comparable to the resonance energy. This results in a large uncertainty in the calculated DR rate coefficient. Barring theoretical advances in this area, laboratory measurements remain the only reliable way to produce the DR data needed for ions forming at these temperatures.

We have incorporated the new DR and RR rate coefficients into our CIE models [8]. Our results differ significantly from the CIE results of Mazzotta et al. [21], which were the previous state-of-the-art for CIE calculations in astrophysics. We find peak fractional abundances that differ by up to 60%. At fractional abundances of 0.1, we find differences of up to a factor of 5. At 0.01, this can increase up to a factor of 11. The peak formation temperature for an ion can shift by up to 20%. Ions with particularly large differences include Mg, Al, Ca, Fe, Co, and Ni.

Figure 7 shows a comparison between our calculated CIE fractional abundances for iron and those of Mazzotta et al. Here we have used recently published AUTOSTRUCTURE calculations for DR [26] and RR [27]. Note that no significant differences between our results and those of Mazzotta et al. are seen for charge states much lower than sodiumlike. This is because the DR and RR data have been updated only for sodiumlike ions and more highly ionized charge states.

We have also carried out CIE calculations using the FAC DR and RR data of refs. 28–30. These results are in good agreement the the AUTOSTRUCTURE-based CIE results. We find that the peak fractional abundance differs by $\leq$10%. At 0.1 fractional abundances, differences are $\leq$30%, and at 0.01 they are $\leq$50%. This reflects the good agreement between the AUTOSTRUCTURE and FAC DR and RR data. Figure 8 shows a comparison between the AUTOSTRUCTURE-based and FAC-based CIE fractional abundances for iron.

Fig. 7. AUTOSTRUCTURE-based CIE results for iron. The continuous-line curves of the upper graph show the ionization fractional abundance as calculated using the AUTOSTRUCTURE DR rate coefficients of ref. 26 for hydrogenlike through sodiumlike ions and the AUTOSTRUCTURE RR rate coefficients of ref. 27 for bare through sodiumlike ions. We use the DR and RR rate coefficients of Mazzotta et al. [21] for ions not calculated in refs. 26 and 27. The EII rate coefficients used are those of ref. 21. The broken-line curves show the abundances calculated by Mazzotta et al. [21]. The lower graph shows the ratio of the calculated abundances. Comparison is made only for fractional abundances greater than 10^{-2}. The lowest ionization stage shown is P-like. We label the AUTOSTRUCTURE-based results as AUTO and those of Mazzotta et al. as Mazz.

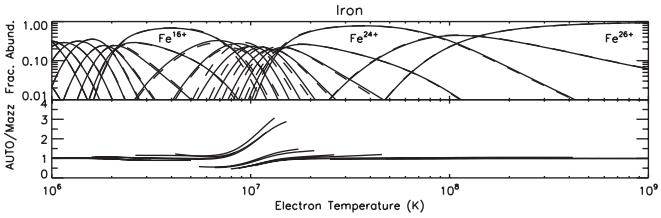

Fig. 8. Comparison with the FAC-based CIE results for iron. The continuous-line curves of the upper graph show the ionization fractional abundance as calculated using the AUTOSTRUCTURE DR rate coefficients of ref. 26 for hydrogenlike through sodiumlike ions and the AUTOSTRUCTURE RR rate coefficients of ref. 27 for bare through sodiumlike ions. The broken-line curves show the abundances as calculated using the FAC DR rate coefficients of refs. 28 and 29 for hydrogenlike through sodiumlike ions and the FAC RR rate coefficients of ref. 30 for bare through fluorinelike ions. We use the DR and RR rate coefficients of refs. 21 for ions not calculated in refs. 26–30. The EII rate coefficients used are those of ref. 21. The lower graph shows the ratio of the calculated abundances. Comparison is made only for fractional abundances greater than 10^{-2}. The lowest ionization stage shown is P-like. We label the AUTOSTRUCTURE-based results as AUTO and the FAC-based results as FAC.

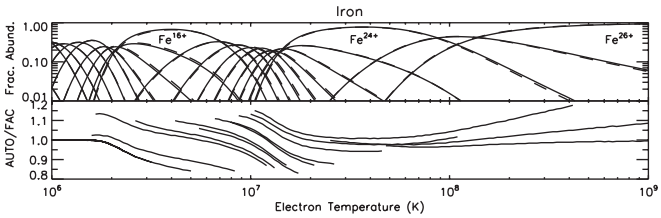

5. CIE Measurements using EBIT MB simulations

EBIT MB simulations can be used to carry out studies of the ionic abundances, and thus of CIE, as a function of electron

temperature. Such measurements have been performed recently at Livermore to measure the charge state distribution of highly charged gold under CIE conditions [31, 32]. A detailed review of these measurements is given by May et al. in these proceedings.

An important aspect of using an EBIT MB simulation to study CIE is to account for the effect of charge exchange (CX) on the ionic abundances. CX involves collisions between ions and neutrals where an electron is captured by the ion from the neutral.

Although the ions in EBIT are trapped by the space charge of the electron beam, the ions leave the immediate confines of the electron beam and can spend a rather large fraction of the time outside the beam. In fact, this ion-beam overlap has been inferred in several ways and may vary between a few percent to near unity [33, 34]. While outside the beam, the ions are subject to interactions with rest gas neutrals and thus to CX. In that case the recombination rate may be much larger than that due to the DR and RR rates assumed in CIE. An EBIT MB simulation can thus only be used to reliably study ionic abundances in CIE if contributions from CX are either minimize and suppressed or accurately known.

To test for the effect of CX on the charge state distribution of gold measured with an MB simulation, measurements were made with different concentrations of background gas. In particular, we varied the amount of argon gas injected into the trap using a gas injector with a precisely controlled continuous flow. The absolute value of the neutral gas density n_0 in the trap is unknown. Also, the actual temperature of the ions and thus their velocity v_i is typically unknown, unless special efforts are made to measure it by very high-resolution crystal spectroscopy [35, 36]. However, a way to measure the product of these two parameters has been devised based on operating an EBIT in the so-called magnetic mode [37], which can be used to detect and account for the presence of CX on the CIE.

In the magnetic mode, the CX-induced X-ray signal decays exponentially as the ions recombine [37]. The exponential decay constant is given by,

$$R_{CX} = n_0 v_i \sigma_{CX} \tag{7}$$

where σ_{CX} is the CX cross section of neutral argon with highly charged gold ions. The neutral gas velocity is assumed negligible compared to the velocity of the trapped ions. Fitting the exponential decay of the X-ray signal during the magnetic mode yields R_{CX}. We then plot the average ionic charge state inferred during the MB simulation, i.e., when the electron beam is on, as a function of R_{CX}. The result is shown in Fig. 9. By interpolating the measurements to a value of $R_{CX} = 0$, the MB simulations yield the average ionic abundance in CIE.

For the particular measurement of gold at a simulated temperature of 2.5 keV shown in Fig. 9, the average ionic charge state did not depend on CX. This result is, however, atypical and may be due to the dominance of dielectronic recombination in this case. In typical situations, the CX recombination rate exceeds that due to RR by factors of five [38].

6. Future modeling needs for MB plasmas in CIE

A significant amount of recombination and ionization data are needed to improve CIE models for astrophysics. We discuss these needs in detail in ref. [8]. Our comments here refer to ions of elements from hydrogen up to and including zinc.

Fig. 9. Average ionic charge of gold for an MB simulation of a 2.5 keV plasma versus the CX rate, R_{CX}.

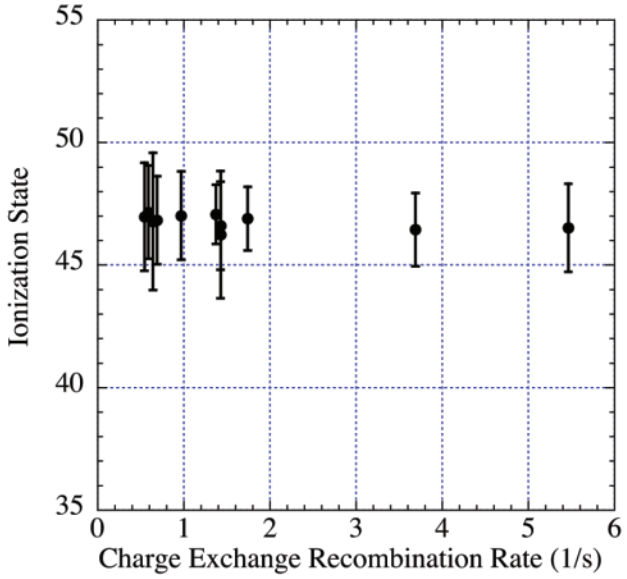

For RR, theoretical and experimental data are needed for M-shell ions of elements up to and including zinc. For DR of L-shell ions, laboratory measurements are needed for boronlike, carbonlike, nitrogenlike, oxygenlike, fluorinelike, and neonlike ions. Modern theoretical calculations exist for these isoelectronic sequences, but there is a paucity of laboratory studies to benchmark the theory. Additionally, as discussed earlier, the reliability of DR theory at temperatures of $\sim 10^4$ K is poor and laboratory data are needed for ions forming at these temperatures. More accurate atomic structure codes could remove much of the uncertainties in the DR theory. More important is the lack of DR for ions with partially filled M-shells. Initial theoretical and experimental work has been carried out for M-shell iron ions [39–41], but significant work remains.

The EII data base used in astrophysics has essentially remained unchanged for almost 20 years. An excellent review of the status of the EII data base is given in ref. 42. In that review, the authors found a factor of 2–3 difference between various recommended published EII data sets (for example, [19, 43]). This is rather surprising as the published data sets all make use of the same few theoretical and experimental results.

An updating of the EII database is sorely needed. Much of the existing data are based on experiments with unknown metastable fractions. The recommended EII data used in astrophysics has not been updated since around 1990. This is partly because few new laboratory measurements or theoretical calculations exist.

CX is both a recombination and an ionization process and is most important for near-neutral systems (charge ≤ 4) [19]. In astrophysics, CX with H is important at temperatures $\lesssim 25\,000$ K [8]. CX in CIE has been investigated in ref. 19. These data need to be updated to reflect recent advances and incorporated into CIE models.

It is clear that vast quantities of data are still needed for reliable CIE models for astrophysics. We propose that these data should be generated with an accuracy of 35% or better.

This is the level of accuracy for the recent state-of-the-art DR and RR calculations and measurements. It would be good if the remaining needed recombination and ionization data were at the same level of accuracy. Additionally, EBIT MB simulations would be quite helpful in testing the current generation of CIE models.

Note added in proof

After this paper was submitted, a re-evaluation and updating of the EII data base was published by Dere [44]. His work points out many instances of discrepancies between EII experiment and theory, indicating that much work remains to resolve these issues. We plan to incorporate these new EII data into our CIE model [8] and will present the results elsewhere.

Acknowledgments

Work at Columbia University was supported in part by a NASA Solar and Heliospheric Physics Supporting Research and Technology grant and an NSF Division of Astronomical Sciences Astronomy and Astrophysics Research grant. Work at Lawrence Livermore National Laboratory (LLNL) and Stanford University was supported in part by a NASA Astronomy and Physics Research and Analysis grant. Work at the University of California LLNL was performed under the auspices of the U.S. Department of Energy under Contract No. W-7405-Eng-48.

References

1. A.L. Osterheld and W.H. Goldstein (*Editors*). Atomic processes in plasmas. Tenth APS topical conference, American Institute of Physics, Melville, New York. 1996.
2. E. Oks and M.S. Pindzola. Atomic processes in plasmas. Eleventh APS topical conference, American Institute of Physics, Melville, New York. 1998.
3. R.C. Mancini and R.A. Phaneuf. Atomic processes in plasmas. Twelfth APS topical conference, American Institute of Physics, Melville, New York. 2000.
4. D.R. Schultz, F.W. Meyer, and F. Ownby. Atomic processes in plasmas. Thirteenth APS topical conference, American Institute of Physics, Melville, New York. 2002.
5. J.S. Cohen, S. Mazevet, and D.P. Kilcreasec. Atomic processes in plasmas. Fourteenth APS topical conference, American Institute of Physics, Melville, New York. 2004.
6. D.W. Savin, P. Beiersdorfer, S.M. Kahn, B.R. Beck, G.V. Brown, M.F. Gu, D.A. Liedahl, and J.H. Scofield. Rev. Sci. Instrum. **71**, 3362 (2000).
7. D.W. Savin, B. Beck, P. Beiersdorfer, S.M. Kahn, G.V. Brown, M.F. Gu, D.A. Liedahl, and J.H. Scofield. Phys. Scr. T, **80**, 312 (1999).
8. P. Bryans, N.R. Badnell, T.W. Gorczyca, J.M. Laming, W. Mitthumsiri, and D.W. Savin. Astrophys. J. Suppl. Ser. **167**, 343 (2006).
9. G.R. Brewer. *In* Focusing of charged particles. *Edited by* A. Septier. Academic Press, New York. 1967. p. 23.
10. J.K. Lepson and P. Beiersdorfer. Phys. Scr. T, **120**, 62 (2005).
11. J. Dubau and S. Volonté. Rep. Prog. Phys. **43**, 199 (1980).
12. A.H. Gabriel. Mon. Not. R. Astron. Soc. **160**, 99 (1972).
13. L.A. Vainshtein and U.I. Safronova. At. Data Nucl. Data Tables, **21**, 49 (1978).
14. L. Steenman-Clark, F. Bely-Dubau, and P. Faucher. Mon. Not. R. Astron. Soc. **191**, 951 (1980).
15. M.H. Chen. At. Data Nucl. Data Tables, **34**, 301 (1986).
16. P. Faucher, M. Loulergue, L. Steenman-Clark, and S. Volonté. Astron. Astrophys. **118**, 147 (1983).
17. H. Zhang and D.H. Sampson. Astrophys. J. Suppl. Ser. **63**, 487 (1987).
18. J.M. Shull and M. van Steenberg. Astrophys. J. Suppl. Ser. **48**, 95 (1982); erratum, **49**, 351 (1982).
19. M. Arnaud and R. Rothenflug. Astron. Astrophys. Suppl. Ser. **60**, 425 (1985).
20. M. Arnaud and J.C. Raymond. Astrophys. J. **398**, 394 (1992).
21. P. Mazzotta, G. Mazzitelli, S. Colafrancesco, and N. Vittorio. Astron. Astrophys. Suppl. Ser. **133**, 403 (1998).
22. A. Müller. *In* Atomic and plasma-material interaction data for fusion, supplement to nuclear fusion. Vol. 6. International Atomic Energy Agency, Vienna, Austria. 1995. p. 59.
23. D.W. Savin and J.M. Laming. Astrophys. J. **566**, 1166 (2002).
24. S. Schippers. Phys. Scr. **80**, 158 (1999).
25. D.W. Savin, G. Gwinner, M. Grieser, R. Repnow, M. Schnell, D. Schwalm, A. Wolf, S.-G. Zhou, S. Kieslich, A. Müller, S. Schippers, J. Colgan, S.D. Loch, N.R. Badnell, M.H. Chen, and M.F. Gu. Astrophys. J. **642**, 1275 (2006).
26. N.R. Badnell, M.G. O'Mullane, H.P. Summers, Z. Altun, M.A. Bautista, J. Colgan, T.W. Gorczyca, D.M. Mitnik, M.S. Pindzola, and O. Zatsarinny. Astron. Astrophys. **406**, 1151 (2003), available from http://amdpp.phys.strath.ac.uk/tamoc/DR
27. N.R. Badnell. Astophys. J. Suppl. Ser. **167**, 334 (2006), available from http://amdpp.phys.strath.ac.uk/tamoc/RR
28. M.F. Gu. Astrophys. J. **590**, 1131 (2003).
29. M.F. Gu. Astrophys. J. Suppl. Ser. **153**, 389 (2004).
30. M.F. Gu. Astrophys. J. **589**, 1085 (2003).
31. K.L. Wong, M.J. May, P. Beiersdorfer, K.B. Fournier, B. Wilson, G.V. Brown, P. Springer, P.A. Neill, and C.L. Harris. Phys. Rev. Lett. **90**, 235001 (2003).
32. M.J. May, P. Beiersdorfer, M. Schneider, S. Terracol, K.L. Wong, K. Fournier, B. Wilson, J.H. Scofield, K.J. Reed, G. Brown, F.S. Porter, R. Kelley, C.A. Kilbourne, and K.P. Boyce. *In* CP770 Atomic processes in plasmas. Fourteenth APS topical conference on atomic processes in plasmas. *Edited by* J.S. Cohen, S. Mazevet, and D.P. Kilcrease. American Institute of Physics, Melville, New York. 2004. p. 61.
33. K.L. Wong, P. Beiersdorfer, R.E. Marrs, B.M. Penetrante, K.J. Reed, J.H. Scofield, D.A. Vogel, and R. Zasadzinski. Nucl. Instrum. Methods, **B72**, 234 (1992).
34. D.R. Dewitt, D. Schneider, M.W. Clark, M.H. Chen, and D. Church. Phys. Rev. A, **44**, 7185 (1991).
35. P. Beiersdorfer, V. Decaux, S.R. Elliott, K. Widmann, and K. Wong. Rev. Sci. Instrum. **66**, 303 (1995).
36. P. Beiersdorfer, V. Decaux, and K. Widmann. Nucl. Instrum. Methods, **B98**, 566 (1995).
37. P. Beiersdorfer, L. Schweikhard, J. Crespo López-Urrutia, and K. Widmann. Rev. Sci. Instrum. **67**, 3818 (1996).
38. P. Beiersdorfer, A.L. Osterheld, M.H. Chen, J.R. Henderson, D.A. Knapp, M.A. Levine, R.E. Marrs, K.J. Reed, M.B. Schneider, and D. A. Vogel. Phys. Rev. Lett. **65**, 1995 (1990).

39. E.W. Schmidt, S. Schippers, A. Müller, M. Lestinsky, F. Sprenger, M. Grieser, R. Repnow, A. Wolf, C. Brandau, D. Lukić, M. Schnell, and D.W. Savin. Astrophys. J. Lett. **641**, L157 (2006).
40. N.R. Badnell. J. Phys. B, **39**, 4825 (2006).
41. N.R. Badnell. Astrophys. J. **651**, L73 (2006).
42. T. Kato, K. Masai, and M. Arnaud. Comparison of ionization rate coefficients of ions from hydrogen through nickel. National Institute for Fusion Science Report, Nagoya, Japan, NIFA-DATA-14. 1991.
43. M.A. Lennon, K.L. Bell, H.B. Gilbody, J.G. Hughes, A.E. Kingston, M.J. Murray, and F.J. Smith. J. Chem. Phys. Ref. Data, **17**, 1285 (1988).
44. K.P. Dere. Astron. Astrophys. **466**, 771 (2007).